WOOD RESEARCH
61 (6): 2016
971-982

A WEIGHTED FILTERED BACK PROJECTION ALGORITHM FOR LOG CT TWO-DIMENSIONAL AND THREE-DIMENSIONAL IMAGE RECONSTRUCTION

Xu Jiahe, Zhou Yucheng, Qi Yuhan, Hou Xiaopeng
Ge Zhedong, Chen Yongping
Chinese Academy of Forestry, Research Institute
of Wood Industry
Beijing, China

(Received January 2016)

ABSTRACT

Log computer tomography (CT) image reconstruction is the kernel of wood CT non-destructive testing (NDT) technology. In this paper, based on the logs physical properties and the X-rays propagation characteristics in solid, the X-ray wave equation inside logs is deduced. A weighted filtered back projection (FBP) algorithm for log CT image reconstruction is proposed. Four group of logs are chosen for simulations on the weighted FBP algorithm. In the two-dimensional image reconstruction process, the capabilities between conventional FBP algorithm and weighted FBP algorithm are compared to verify the effectiveness of the algorithms for logs of different species. From both the image quality and data results, it can be clearly seen that the weighted FBP algorithm has good performance and advantages for image reconstruction process of log CT scan. The three-dimensional log image reconstruction is well completed, but has a big room for improvement.

KEYWORDS: Log, filtered back projected (FBP), image reconstruction, computer tomography (CT), non-destructive testing (NDT).

INTRODUCTION

Wood nondestructive testing (NDT) technology is an emerging technology applied in wood and wood materials detection, by which wood can be detected and processed effectively, and then the physical properties, defects and internal information of wood can be judged (Wang et al. 2001a). NDT techniques have been widely used wood construction materials, in terms of ancient building protection also by means of NDT technology (Duan et al. 2002). After decades of development, the physical properties of wood-based panels and wood have been detected utilizing

computer tomography (CT), ray method, infrared method and microwave method (Bucur and Archer 1984, Lindgren 1991, Ouis 2000, Tsuchikawa et al. 2000, Wang et al. 2001b).

CT technology is an imaging technology by ray projection measure on objects with different angle to obtain cross-sectional information of the object (Yu and Gong 2015). CT technology is widely used in the medical and industrial fields. Similarly, the basic principles of CT technology applied to the forest products industry is also make use of the ray projection data between attenuation and density in each direction of the object, to reconstruct image. Human organ composition position and tissue density are relatively fixed, while the wood composition, density, moisture content, internal defect are ever changing (An et al. 2008). Thus, while CT technology has been proven it can solve the conventional optical imaging, and is widely used in many important fields of biomedical and industrial NDT, but because of the reconstruction difficulty caused by scattering photons in turbid medium of wood, it faces a tough challenge for log deep tissue images reconstruction.

In the process of CT imaging formation, the kernel is the algorithm of projection image reconstruction theory (Yan and Li 2015), whereby efficient and scientific methods of projection image reconstruction are particularly important to improve the CT reconstruction image quality and detection accuracy. In the fan-beam CT scan, the most common image reconstruction algorithm is Filtered Back Projection (FBP) algorithm (Shi and Luo 2013, Zheng et al. 2013, Bilgot and Desbat 2011), which carries out convolution with one-dimensional ramp filter operator and projection data, superimposes projection data in all horizontal directions, and reconstruct two-dimensional image of fracture surface.

Although the FBP technique can be useful when solving time dependent partial differential equations using Fourier spectral methods, the image quality can be further improved. For example, the kernel for the FBP algorithm, choose of filtered operator, has been usually based on empirical expressions. Many window functions (Chesler and Riederer 1975, Hamming 1977, Butterworth 1930) in the Fourier domain have been suggested to suppress the reconstruction image noise. Recently, window functions have been derived to compensate for the projection noise on the ray-by-ray base (Zeng and Zamyatin 2013). Despite compelling numerical evidence, there is no general expression to show the range of restrictions by using window functions in Fourier domain for different sampling frequency.

In this paper, a weighting function is disclosed for image reconstruction of log CT detection. An adaptive criterion has been derived from the X-ray wave equation. Numerical simulation results for scanning logs from different varieties of trees demonstrates the effectiveness of the proposed log CT image reconstruction algorithm.

During scanning logs, transmission data are created inside a tissue after it absorbs energy, which can be used to reconstruct two-dimensional (2D) and three-dimensional (3D) images of the tissue. The basic physics background and mathematical formula for the X-ray wave and propagation are deduced below.

Wave equations

Logs belong to nonmagnetic and semi-insulator material, the X-rays wave equation inside logs can be obtained from the material equations and material equations by:

$$\nabla^2 E - \frac{1}{c^2}\frac{\partial^2 E}{\partial t^2} = \frac{1}{\varepsilon_0 c^2}\frac{\partial^2 P}{\partial t^2} \tag{1}$$

where: E - electric field intensity,
ε_0 - dielectric coefficient in vacuum,
P - polarization intensity of medium,
c - speed of light in vacuum.

Here, right-hand side of above equation is extremely important polarization term, which can interpret absorption and dispersion and other optical effects resulted in ray attenuation in logs interior, in which the charge of *P* generated by the polarization charge over time reflect the change of electric displacement over time. And it can be given that,

$$\frac{\partial P}{\partial t} = I(r,t) \tag{2}$$

where: *I(r,t)* - the time dependent energy attenuation (Li 2011).

Putting Eq. (2) into Eq. (1) gives:

$$\nabla^2 E - \frac{1}{c^2}\frac{\partial^2 E}{\partial t^2} = \frac{1}{\varepsilon_0 c^2}\frac{\partial I(r,t)}{\partial t} \tag{3}$$

In most experimental conditions, it is applicable to consider the incident laser pulse having a Gaussian profile with the absorbed energy given by:

$$I(r,t) = I(r)\cdot\frac{\exp(t^2/2\tau^2)}{\tau} \tag{4}$$

where: τ - a characteristic time. From the definition of

$$\delta(x) = \lim_{n\to\infty}\sqrt{\frac{n}{\pi}}e^{-nx^2} \tag{5}$$

X-ray as a very short wavelength laser pulses, is short enough so that the density of the log sample has no time to change, the energy attenuation function can be modeled as a Dirac delta function, given by:

$$I(r,t) = I(r)\delta(t) \tag{6}$$

Under this condition, the X-ray vector field equation can be written as:

$$\frac{\partial I(r,t)}{\partial t} = I(r)\frac{\partial \delta(t)}{\partial t} \tag{7}$$

From the above analysis, under this condition, the photoacoustic wave equation can be written as:

$$\nabla^2 E(r,t) - \frac{1}{c^2}\frac{\partial^2 E(r,t)}{\partial t^2} = \frac{1}{\varepsilon_0 c^2} I(r)\frac{\partial \delta(t)}{\partial t} \tag{8}$$

Weighting function in fourier space

From the equation (8), it can be seen that is active time-dependent Helmholtz equation. For log CT image reconstruction, we need to consider how to solve the Helmholtz equation. In infinite space, as long as the solution of Green function equation corresponding to the above-mentioned Helmholtz equation is obtained, we can get solution of Helmholtz equation. Thus, in the following, we will discuss the 2D and 3D solution of Green function equation corresponding to Helmholtz equation respectively.

Two-dimensional solution of Green function equation

The derivation will start from the equation (8). Fourier transform of the equation (8) is given by:

$$\tilde{G}_{2D}(k,\omega) = \frac{e^{-i(kr+\omega t)}}{k^2+\omega^2+\frac{1}{c^2}} \tag{9}$$

For t>0, the inverse Fourier transform of the equation (9) can be calculated based on Cauchy's residue theorem:

$$G_{2D}(r,r',t)=\frac{c}{4\pi}\int\frac{\sin(ckt)}{k}e^{-ik(r-r')}dk \tag{10}$$

In order to further derive the solution for the wave equation inside logs, the following mathematical substitutions are first utilized:

$$\int\delta'(t-t_0)f(t)dt=-f'(t_0)\quad\text{and}\quad\frac{\partial G}{\partial t'}=-\frac{\partial G}{\partial t} \tag{11}$$

The wave equation (8) has a general solution that can be expressed as:

$$E(r,t)=\frac{1}{\varepsilon_0 c^2}\int_S I(r')\frac{\partial G_{2D}(r,r',t)}{\partial t}d^2r' \tag{12}$$

which results in:

$$\frac{\partial G_{2D}(r,r',t)}{\partial t}=\frac{c^2}{4\pi}\int\cos(ckt)e^{-ik(r-r')}dk \tag{13}$$

E(r, t) can be further derived by utilizing the above equation.

Therefore, the initial X-ray energy source function in time domain can be expressed as:

$$E_{2D}(r,t)=\frac{1}{4\pi\varepsilon_0}\int_{-\infty}^{+\infty}E(k,t)W(k,r,t)e^{-ik\square r}d^2k \tag{14}$$

where: $W(k,r,t)=\dfrac{e^{-2ik\square r}}{\cos(ckt)}$.

Three-dimensional solution of Green function equation

Let source located at the origin (0, 0, 0), the physical meanings of solving Helmholtz equation in Cartesian coordinates is: spherical wave can be converted into a superposition of cylindrical wave.

The resulting Green's function under three-dimensional conditions can be given by:

$$G_{3D}(r,r',t,t')=\frac{\delta(|r-r'|-c(t-t'))}{4\pi|r-r'|} \tag{15}$$

The same mathematical substitutions (3.3) are utilized, the wave equation (2.8) has a general solution that can be expressed as:

$$E(r,t)=\frac{1}{\varepsilon_0 c^2}\int_V I(r')\frac{\partial G_{3D}(r,r',t)}{\partial t}d^3r' \tag{16}$$

From the inverse Fourier transform of Green's function, the following can be obtained:

$$G_{3D}(r,r',t,t')=\frac{1}{(2\pi)^4}\iint\frac{e^{-ik(r-r')}e^{j\omega(t-t')}}{k^2-(\omega/c)^2}d\omega d^2k \tag{17}$$

For the frequency axis, it can be seen that there are two simple poles when $\omega=\pm ck$ because:

$$\frac{e^{-ik(r-r')}e^{j\omega(t-t')}}{k^2-(\omega/c)^2}=\frac{e^{-ik(r-r')}e^{j\omega(t-t')}}{(k+\omega/c)(k-\omega/c)} \tag{18}$$

Similarly, it can be further derived by utilizing the above equation. Therefore, the initial X-ray energy source function in time domain can be expressed as:

$$E_{3D}(r,t) = \frac{1}{\varepsilon_0 (2\pi)^3} \int_k E(k,t) W(k,r,t) e^{-ik\square r} d^3k \tag{19}$$

where: $W(k.r.t) = \dfrac{e^{-2ik\square r}}{\cos(ckt)}$.

Remarks for weighted filtered back projection algorithm

This weighting function has a rigorous form directly derived from the wave equation inside logs. Equations (14) and (19) only differ in the number of dimensions. In the three-dimensional case, the acquired data are two-dimensional projections through the sample. It can be seen that both the weighting functions represent the amount of contributions from a signal E(k,t) for the image reconstruction in the Fourier domain. The conventional FBP algorithms require multiplying Fourier transform of projection data by a product of an absolute linear variable, using window functions for filtering the projection data, and then back projecting data which are treated in time domain, of which ramp-filtering can be implemented as multiplication in the frequency domain or as convolution in the spatial domain. In the weighted FBP algorithm, a weighting function is used in Fourier space, this weighting function allows a clear reconstruction image to be constructed without using an artificial filter for logs, i.e., without using empirically selected window functions in Fourier space.

In the derivation process, since the permittivity and conductivity and other parameters of logs are affected by the wood structure, moisture content, density, temperature and direction of the fibers and so on, the exact relationship between substance parameters of logs and image reconstruction algorithm cannot be accurately determined, therefore, we consider to translate the polarization intensity into energy attenuation of logs for derivation, and not directly reflect the permittivity and conductivity of logs in the equations. However, whether these assumptions and ignores will affect the quality and accuracy of reconstructed images, we did not know. The relationship between the two needs to be verified by a large number of test demonstrations, merely from the derivation is difficult to judge.

Therefore, in the next section of this article, we choose in two kinds of coniferous woods and two kinds of broad-leaved woods for simulations, to verify the effectiveness of the algorithm, which provide more sufficient and favorable evidence for the weighted filter back projection algorithm able to better adapt to log CT detection image reconstruction of different species.

MATERIAL AND METHODS

The actual algorithms for back projection use a trick for the reconstruction in order to simplify the computation burden of image reconstruction process. We do not need to numerically integrate the back projection equations of the 2D (14) and the 3D (19) back propagation algorithms. Instead, we identify the fast Fourier transform for *E(r, t)* used to speed up the computation and perform the reconstruction projection-wise for each rotational position θ.

Log CT equipment, developed by our project team, is used in the scanning, detection and data acquisition of the simulation, the hardware structure chart shown in Fig. 1. The entire system completes ray scan data acquisition of the experiment logs centered on the computer.

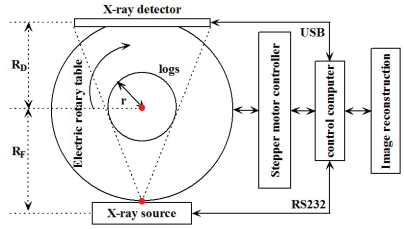

Fig. 1: The hardware structure of log CT equipment.

Set the X-ray source tube voltage of 120 kV, tube current of 60 mA, X-ray detector channels of 1280, the sampling integration time of 1 ms. From the center of the rotary table to the focus of X-ray source is 566 mm, X-ray source to detector distance is 895 mm, the system magnification M is 1.58, and the system spatial resolution is 0.39 mm.

Four groups of cylindrical logs are chosen as the experimental subjects for scanned data acquisition, where Cedarwood (*Cunninghamia lanceolata*) and Dahurian larch (*Larch gmelini*) are two kinds of coniferous wood; and Locust (*Robinia pseudoacacia*) and Sassafras (*Sassafras tzumu*) are two kinds of broad-leaved wood, in which Sassafras is also ring-porous wood. The data and pictures of experimental logs shown in Tab. 1 and Fig. 2 respectively.

Tab. 1: The data of experimental logs.

Name	Cedarwood	Locust	Dahurian larch	Sassafras
Diameter (cm)	24	22	19	22
Height (cm)	9	12	6-8	27
Moisture content	7.9 %	8.9 %	9.6 %	8.0 %
Scanning time (min)	7.85	8.23	6.39	17.17
Actual tube current value (mA)	62	63	66	61

a) Cedarwood (Cunninghamia lanceolata) b)Locust (Robinia pseudoacacia)

c) Dahurian larch (Larch gmelini) d) Sassafras (Sassafras tzumu)

Fig. 2. The pictures of experimental logs: a) Cedarwood (Cunninghamia lanceolata); b) Locust (Robinia pseudoacacia); c) Dahurian larch (Larch gmelini); d) Sassafras (Sassafras tzumu).

In order to test the weighted FBP algorithm, numerical simulations were conducted on phantom samples, where the variance of the non-stationary Gaussian noise is determined by the exponential relationship as $\sigma_i^2=f_i*exp(E_i\,\eta)$, where, set f_i = 100, η=22.000.

RESULTS AND DISCUSSION

Filter back projection algorithm

In FBP algorithm, the filtered function has great influence on the quality of the image reconstruction (Huang et al. 2012). Commonly, conventional filter functions include R-L filter function (Ramachandran and Lakshminarayanan 1971), S-L filter function (Shepp and Logan 1974), etc., each with its advantages and disadvantages. In order to improve the quality of image reconstruction, hybrid filter functions are also proposed (Zeng 2015). Hybrid filter functions take into account both spatial resolution and density resolution of the reconstructed images, and have good image noise suppression. In this paper, the popular RL-SL hybrid filter function is chosen.

Using the conventional FBP algorithm to complete image reconstruction with log CT scan data, the resulting images are shown in Fig. 3.

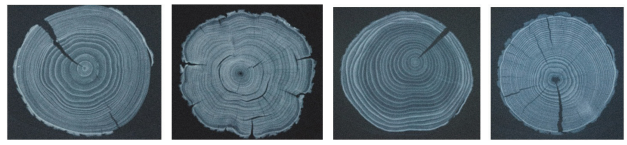

a) *b)* *c)* *d)*

Fig. 3: The image reconstruction results of four groups of experimental logs by conventional filtered back-projection algorithm: a) Cedarwood (Cunninghamia lanceolata); b) Locust (Robinia pseudoacacia); c) Dahurian larch (Larch gmelini); d) Sassafras (Sassafras tzumu).

Two-dimensional weighted back projection algorithm

From Fig. 3, it is shown that the conventional FBP algorithm with the choice of RL-SL hybrid filter function for log CT image reconstruction process can reflect the internal situation of logs, including cracks and growth rings. However, since the noise is added to the simulation data, we will further comparison algorithms on the abilities of noise proof and noise filtration. From Fig. 3, it can be seen that there are obvious noises in the image, for the growth rings or the experimental logs with obscure boundary; it has interfered with the judgment of the rings and borders.

Two-dimensional weighted back projection algorithm

To implement the algorithm, we introduce a one-dimensional inverse fast Fourier transform FFT_{10}^{-1} and a discrete sum over N equidistant projections firstly.

Using the proposed weighted FBP algorithm for two-dimensional image reconstruction with the CT scan data, the resulting images are shown in Fig. 4. It is seen from Fig. 4, the weighted FBP algorithm for log image reconstruction process can well reflected the internal situation of logs, including cracks and growth rings. At the same time, while also adding noise in the simulation data, we found that the weighted FBP algorithm has better capabilities of noise proof and noise filtration. Seen from Fig.4, there is no obvious noise in the image, for the growth rings or the experimental logs with obscure boundary; images can clearly reflect the state of the growth rings and boundaries.

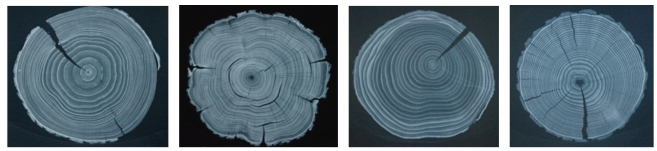

a) *b)* *c)* *d)*

Fig. 4: The two-dimensional image reconstruction results of four groups of experimental logs by the weighted filtered back-projection algorithm: a) Cedarwood (Cunninghamia lanceolata); b) Locust (Robinia pseudoacacia); c) Dahurian larch (Larch gmelini); d) Sassafras (Sassafras tzumu.

In order to compare the quality of image reconstruction algorithms more clearly, we deal with two groups of images enlarged, as shown in Fig. 5. From Fig. 5, we can clearly compare the sharpness and denoise effect of the two reconstruction images, the weighted FBP algorithm has obvious advantage on log CT image reconstruction.

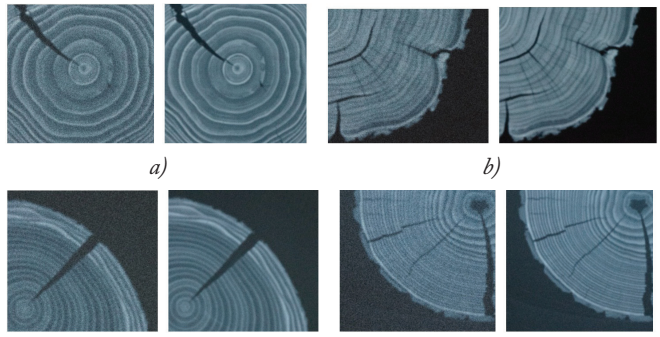

a) *b)*

c) *d)*

Fig. 5: The two-dimensional image reconstruction locality comparisons of four groups of experimental logs between conventional filtered back-projection algorithm and the weighted filtered. back-projection algorithm: a) Cedarwood (Cunninghamia lanceolata); b) Locust (Robinia pseudoacacia); c) Dahurian larch (Larch gmelini); d) Sassafras (Sassafras tzumu).

Furthermore, we implement quantitative comparison between the two groups of reconstruction images, and further verify the performance of the two algorithms. The reconstruction time data of four groups of experimental logs are given, and the image noise estimation variance of the reconstructed image in Figs. 3 and 4 are compared in Tab. 2.

Tab. 2: The comparison of reconstruction time and estimation noise variance between conventional filtered back-projection algorithm and the weighted filtered back-projection algorithm.

		Reconstruction delay time (s)	**Estimation noise variance**
Conventional filtered back projection algorithm	Cedarwood	9.72	25.0131
	Locust	8.02	24.9645
	Dahurian larch	9.30	24.9859
	Sassafras	9.69	25.0563

Weighted filtered back projection algorithm	Cedarwood	5.23	5.0317
	Locust	4.37	5.0054
	Dahurian larch	5.09	4.9167
	Sassafras	5.11	5.1627

In a word, from both the image quality and data results, it can be clearly seen that the weighted filtered back-projection algorithm has good performance and advantages for image reconstruction process of log CT scan.

Furthermore, in the hierarchical scan process of experimental sassafras, when we carry out reconstruction of scanning layers on different height, we find there are many nodules inside this log, as shown in Fig. 6.

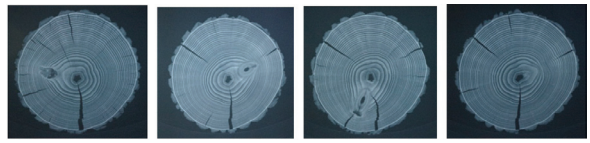

a) *b)* *c)* *d)*

Fig. 6: The reconstruction images on different layer of the precise hierarchical scan on the experimental sassafras: a) the 75 layer; b) the 180 layer; c) the 245 layer; d) the 290 layer.

In order to facilitate the subsequent three-dimensional imaging, we carry out precise hierarchical scan on this sassafras. The height of whole sassafras is 27 cm, we obtain 290 layers from the bottom to top with the interval of 0.75 mm. We find three distinct nodules at different heights: the first nodule presents at 50-85 layers with 4 cm long (Fig. 6 a); the second nodule presents at 150-210 layers with 6 cm long (Fig. 6 b); the third nodule presents at 220-275 layers with 3.5 cm long (Fig. 6 c); to the top of the 290 layer exhibits well log cross section (Fig. 6 d).

Three-dimensional weighted back projection algorithm

Here, we use a two-dimensional Fourier transform FFT_{2d}^{-1} . Using the proposed weighted FBP algorithm to further 3D image reconstruction with log CT scan data, four groups of 3D reconstruction image of experimental logs are shown in Figs. 7 to 10. From the figures, it is shown that the weighted FBP algorithm for log 3D image reconstruction process can be obtained, including cracks and growth rings and barks.

However, the weighted FBP algorithm for 3D image reconstruction of logs still has many problems: Firstly, since the three-dimensional imaging principle of the weighted FBP algorithm adopts the way of multi-layer stack, leading to mutual interference between the layers image in overlay process, the appearances of blurring boundaries or growth rings exist in the superimposed three-dimensional images, as shown in Figs. 7 and 8; secondly, in the process of three-dimensional imaging, when the log has complex internal structure, the presence of coupling between the image reconstruction data results in indistinct image reconstruction manifestation, even strip artifacts, as shown in Fig. 9; Finally, since the multi-image superposition, many irregularities structures comprising inside the logs are covered and obscured by the outer image, the internal states of logs cannot be clearly shown, as shown in Fig. 10. Fig. 10 is the 3D imaging results of sassafras that specifically mentioned in the 2D imaging process, in the 2D hierarchical scan imaging, we have mentioned there are three nodules of different lengths at different locations in the experimental Sassafras interior, however in the 3D imaging, three nodules hidden inside are covered and obscured by the outer image, we cannot clearly see the status of the internal nodule.

Thus it can be seen the weighted FBP algorithm for log 3D image reconstruction still exists room for further improvement.

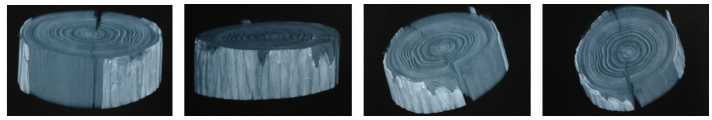

Fig. 7: The three-dimensional image reconstruction results of experimental Cedarwood (Cunninghamia lanceolata) logs by the weighted filtered back-projection algorithm.

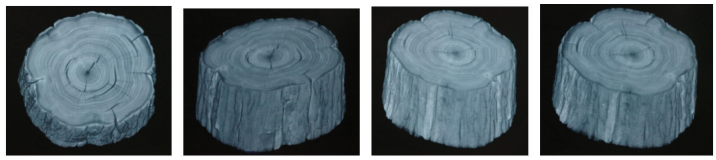

Fig. 8: The three-dimensional image reconstruction results of experimental Locust (Robinia pseudoacacia) logs by the weighted filtered back-projection algorithm.

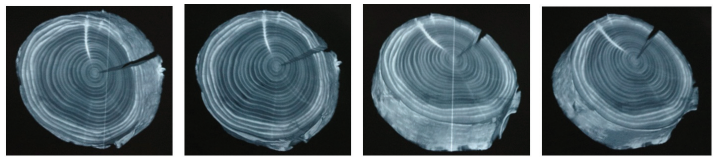

Fig. 9: The three-dimensional image reconstruction results of experimental Dahurian larch (Larch gmelini) logs by the weighted filtered back-projection algorithm.

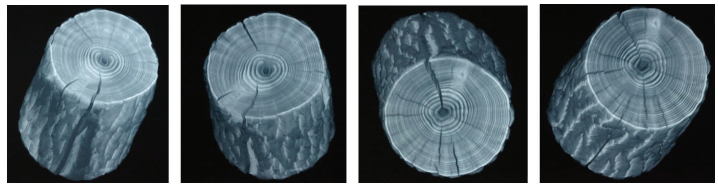

Fig. 10: The three-dimensional image reconstruction results of experimental Sassafras (Sassafras tzumu) logs by the weighted filtered back projection algorithm.

CONCLUSIONS

In this paper, based on the physical properties of logs and the X-rays propagation characteristics in solid, the X-ray propagation wave equation inside logs is provided. On the strength of the wave equation, the complete weighted filtered back projection algorithm for two-dimensional and three-dimensional image reconstruction of log CT detection is proposed.

The proposed weighted FBP algorithm is directly derived from the X-ray wave equation inside logs, mainly applied to the image reconstruction and image processing of log CT detection. The conventional FBP algorithm requires multiplying an absolute linear variable to increase the Fourier transform of projection data. However, the weighted function allows image reconstruction without using an empirically selected artificial filter for logs in Fourier space.

We chose two kinds of coniferous woods and two kinds of broad-leaved woods as the

experimental subjects for scanned data acquisition. In the two-dimensional image reconstruction process, by a method of adding artificial noise, compared to the capabilities of noise proof and noise filtration between conventional FBP algorithm and weighted FBP algorithm. Through analysis of specific image and noise data, it can be seen that the proposed weighting FBP algorithm is more suitable for log CT NDT image reconstruction, which has higher precision of reconstruction image and better noise filtering effect. In the three-dimensional image reconstruction process, although the overall image reconstruction is well, but after analysis of each reconstructed image, it is shown the weighted FBP algorithm for log three-dimensional image reconstruction and image process has a big room for improvement.

The proposed weighted FBP algorithm will become a feasible and flexible tool in modern CT detection image reconstruction for better adapting to the logs of different species and different regions.

ACKNOWLEDGMENTS

This work is supported by the Forestry Projects in the central level public welfare scientific research institutes basic scientific research business special funds CAFYBB2014QA019, the Forestry Projects in the central level public welfare scientific research institutes basic scientific research business special funds CAFYBB2016QA010, and the National Natural Science Foundation of China 31570711.

REFERENCES

1. An, Y., Yin Y., Jiang X., 2008: Inspection of decay distribution in wood column by stress wave and resistograph techniques. Journal of Building Materials 11(4): 457-463 (in Chinese).
2. Bilgot, A., Desbat, L., 2011: Valerie Perrier. FBP and the interior problem in 2D tomography. In: Proceedings of the 2011 IEEE Nuclear Science Symposium and Medical Imaging Conference. Pp 4080-4085, IEEE Press, Piscataway.
3. Bucur, V., Archer, R.R., 1984: Elastic contants for wood by an ultrasonic method. Wood Science and Technology 18(4): 255-265.
4. Butterworth, S., 1930: On the theory of filter amplifiers. Experimental Wireless and the Wireless Engineer 7: 536-541.
5. Chesler, D.A., Riederer, S.J., 1975: Ripple suppression during reconstruction in transverse tomography. Physics in Medicine and Biology 20(4): 632-636.
6. Duan, X.F., Li, Y.D, Wang, P., 2002: Review of NDE technology as applied to wood preservation. China Wood Industry 16(5): 14-16.
7. Hamming, R.W., 1977: Digital filters. Prentice Hall. Englewood Cliffs, 226 pp (in Chinese).
8. Huang, Y., Zhang, X.Z., Zhu, J.W., Liu, H.G., Tai, R.Z., 2012: A new type of filter function for CT image reconstruction. Nuclear Electronics and Detection Technology 32(12): 1388-1393 (in Chinese).
9. Li, Y.Q., 2011: Medical imaging theory. People's Medical Publishing House. Beijing, 38 pp.
10. Lindgren, L.Q., 1991: Medical CAT-scanning: X-Ray absorption coefficients, CT-numbers and their relation to wood density. Wood science and Technology 25: 341-349.

11. Ouis, D., 2000: Detection of decay in logs through measuring the dampening of bending vibrations by means of a room acoustic technique. Wood Science and Technology 34(3): 221-236.
12. Ramachandran, G.N., Lakshminarayanan, A.V., 1971: Three-dimensional reconstructions from radiographs and electron micrographs: Application of convolution instead of Fourier transforms. In: Proceedings of the National Academy of Sciences 68(9): 2236-2240.
13. Shepp, L.A., Logan, B.F., 1974: The Fourier reconstruction of a head section. IEEE Transactions on Nuclear Science 21(3): 21-43.
14. Shi, H.L., Luo, S.Q., 2013: A novel scheme to design the filter for CT reconstruction using FBP algorithm. Bio Medical Engineering Online 12(1): 1-15.
15. Tsuchikawa, S., Takahashi, T., Tsutsumi, S., 2000: Nondstructive measurement of wood properties by using near-infrared laser radiation. Forest Products Journal 50(1): 81-86.
16. Wang L.H., Yang X., Xu K., 2001a: Current situations and research development of non-destructive testing for wood properties. Forest Engineering 17(6): 1-3.
17. Wang, J., Biernacki, J., Lam, F., 2001b: Nondestructive evaluation of veneer quality using acoustic wave measurement. Wood Science and Technology 34(6): 505-516.
18. Yan, B., Li, L., 2015: CT image reconstruction algorithm. Science Press. Beijing, 3 pp.
19. Yu, X.E., Gong, J., 2015: CT principle and technology. Science Press. Beijing, 2 pp.
20. Zeng, G.L., Zamyatin, A., 2013: A filtered back projection algorithm with ray-by-ray noise weighting. Medical Physics, Medical Physics 40(3): 031113.
21. Zeng, G.L., 2015: Revisit of the ramp filter. IEEE Transactions on Nuclear Science 62(1): 131-136.
22. Zheng, F., Xin, G., Xing, L.Z., Jing, R.Z., Si, Y.C., 2013: Research on the relationship between projection number and image noise level in FBP reconstruction. Advanced Materials Research 718/719/720: 2324-2328.

*Xu Jiahe, Zhou Yucheng, Qi Yuhan, Hou Xiaopeng
Ge Zhedong, Chen Yongping
Chinese Academy of Forestry
Research Institute of Wood Industry
Beijing 100091
China
Correspoding author: ellipisis@qq.com